PACS numbers: 74.20.Mn, **74.72.–h**
DOI: 10.1070/PU2008v051n02ABEH006468
DOI: 10.3367/UFNr.0178.200802i.0202

With cuprate luggage to room-temperature superconductivity

Yu V Kopaev, V I Belyavsky, V V Kapaev

1. Problems and progress in the physics of cuprates

The high-temperature superconductivity (HTSC) of cuprates was discovered in 1986 [1], when the highest superconducting transition temperature characteristic of conventional superconductors ($T_c = 23.2$ K in Nb_3Ge) was substantially exceeded and a superconducting (SC) transition temperature $T_c \approx 30$ K was achieved in the ceramic $La_{2-x}Ba_xCuO_{4+\delta}$. Within a year after this discovery, the record value of T_c exceeded 90 K ($YBa_2Cu_3O_{6+\delta}$ ceramic). The further search for and creation of new SC materials led to $T_c = 138$ K (Tl-doped $HgBa_2Ca_2Cu_3O_{8+\delta}$ compound) in 1994 and raised the question of room-temperature superconductivity.

Studies over the last two decades have not brought researchers to agreement concerning the superconductivity mechanism in cuprate compounds and have not resulted in a theory similar to the Bardeen–Cooper–Schrieffer (BCS) theory of conventional superconductors [2]. Nevertheless, we must acknowledge significant progress in understanding the nature of cuprate superconductivity that has been achieved in these years.

The key structural element of layered quasi-two-dimensional (2D) cuprates is a (CuO_2) plane (one or several in a unit cell); they differ from conventional superconductors not only in high values of T_c but also in a set of physical properties that cannot be described by the BCS scheme. In cuprates, charge carriers appear due to the doping of the CuO_2 planes of a parent antiferromagnetic (AF) insulator upon nonisovalent atomic substitution or the creation of oxygen vacancies in charge reservoirs outside the conducting planes. The distance between equivalent CuO_2 planes in neighboring unit cells is large compared to the in-plane distance between neighboring copper atoms, which results in a strong conductivity anisotropy at temperatures above T_c and the 2D coherence of the SC state at temperatures below T_c.

In the absence of an external magnetic field, the thermodynamic state of a doped cuprate compound can be described by the temperature T and the carrier concentration in the CuO_2 plane (doping level) x. In the phase diagram (Fig. 1), the SC state field corresponds to a certain doping range $x_* < x < x^*$ inside which the SC transition temperature reaches its maximum value at the optimum doping x_{opt}. Concentrations $x \lesssim x_{opt}$ correspond to underdoped cuprates, and concentrations $x \gtrsim x_{opt}$ to overdoped cuprates.

At $x \gtrsim x_{opt}$ and $T > T_c$, cuprates are 'bad' Fermi liquids, and at $x \lesssim x_{opt}$, over a wide temperature range $T_c < T < T^*$, they exhibit the pseudogap state, whose nature is still unknown [3]. The gap spectrum of quasiparticles at $T > T_c$ demonstrates that the SC phase appears from a certain insulating state rather than from a Fermi liquid, such that the ground states of an insulator and a superconductor, with similar structures and energies, converge near the SC transition line. This behavior corresponds to the concept of strong correlations in cuprates, which result in the competing singlet states of a d-wave superconductor and a flux insulating phase [4].

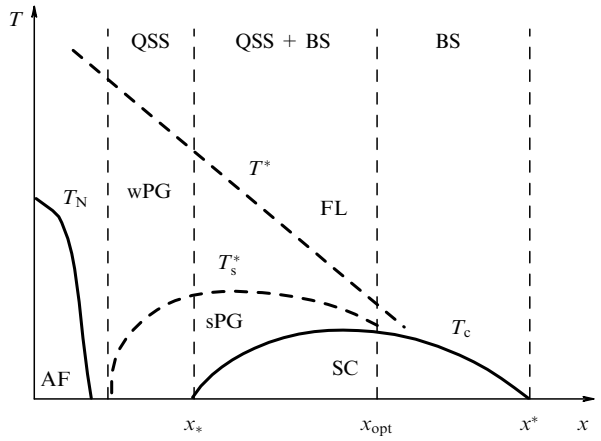

Figure 1. Typical phase diagram of hole-doped cuprates. The Néel (T_N) and SC transition (T_c) temperatures respectively bound the long-range AF and SC order regions. Strong pseudogap (sPG) and weak pseudogap (wPG) regions are separated by a crossover temperature T_s^*. The temperature T^* separates the weak pseudogap from the normal Fermi liquid (FL). The regions in which the bound states (BSs) and quasi-stationary states (QSSs) of K pairs appear are shown, and the region of coexisting BS and QSS is also depicted.

The pseudogap state is divided into a strong pseudogap that is adjacent to T_c and exists over a wide temperature range $T_c < T \lesssim T_s^*$, and a weak pseudogap between T_s^* and T^*. The strong pseudogap has a high nonlinear diamagnetic response [5, 6] and a giant Nernst effect [7] and can be related to a fluctuating SC order in the form of noncoherent long-lived quasi-stationary states of SC pairs [8]. T_s^* corresponds to the breaking of a pair, and T_c corresponds to the appearance of phase coherence in the system of pairs. A consistent theory of cuprate superconductivity should be able to explain both the high values of T_c and the physical properties of these compounds in a large neighborhood of the SC state that includes the strong and weak pseudogaps in the phase diagram.

Strong electron correlations and the unusual symmetry of the pseudogap and the SC order parameter in cuprates are arguments for a purely electron superconductivity mechanism (rather than a phonon mechanism, as in the BCS theory). The studies of this mechanism for strong intracenter Coulomb repulsion in terms of the Hubbard model and the related $t-J$ model are described in a number of reviews [9]. The 2D Hubbard problem has not been exactly solved, and approximate solutions obtained by numerical methods are often in conflict, which leads to reasonable doubts about the usefulness of this approach [10], especially because the unusual isotopic effect in cuprates [11–13] indicates a nontrivial role of phonons in pairing-interaction formation.

For pairing repulsion, the singlet SC order parameter $\Delta(\mathbf{k})$ is a scalar function of the momentum $\mathbf{k}$, and this function should be alternating in its domain after the separation of the phase factor corresponding to the center-of-mass motion of the pair. An analysis of experiments sensitive to the momentum dependence of the order parameter [14, 15] demonstrates that $\Delta(\mathbf{k})$ vanishes at several points in the Fermi contour (FC) that can correspond to an extended s or s + g symmetry ($\Delta(\mathbf{k})$ does not change its sign under rotation through the angle $\pi/2$) or a d symmetry (four zeros as a result of the change in the sign of $\Delta(\mathbf{k})$ upon rotation through the angle $\pi/2$).

Order-parameter zeros open a channel for scattering by nonmagnetic impurities, which is ineffective for the s symmetry and corresponds to the BCS phonon mechanism. This should break the SC state, whose resistance to scattering by nonmagnetic impurities is one of the key tests for a cuprate superconductivity theory.

This theory should explain a number of specific features of cuprates that distinguish them from conventional superconductors. For example, the optical-conductivity measurements in [16] demonstrate that upon SC condensation, the spectral weight is redistributed over a wide energy range $\gtrsim 100\Delta$ rather than in an energy range $\sim \Delta$, as follows from the BCS theory (the high-energy problem [17]). Moreover, the real part of the optical conductivity exhibits the Drude behavior $\sigma_1 \sim \omega^{-2}$ for $T < T_c$; that is, the particle density in the SC condensate is comparable to the density of off-condensate particles. The same conclusion follows from the temperature dependence of the heat capacity [18], which corresponds to a gap-free spectrum of elementary excitations at $T < T_c$, $c_V \sim T$. The key problems of the physics of cuprates also involve the origin and role of the self-organization of an electron system in the form of stripes [19] or the staggered spatial ordering of the system at $T < T_c$ (in the form of an SC-pair density wave [20]).

Although modern approaches to the problem of cuprate superconductivity are often based on different physical concepts (such as the traditional phonon mechanism [21], the resonating valence bond (RVB) scheme [22, 23], the SU(2) charge–spin separation scheme [4], the concept of high-momentum SC pairing [8], the theory of an algebraic Fermi liquid [24], the concept of a quantum critical point [25], and the SO(5) phenomenology [26] or the SU(4) phenomenology [27]), their consequences have many common features [28]. The usefulness of a certain approach is determined by its ability to explain the properties of HTSC compounds and to suggest ways to increase their critical parameters [17].

2. Superconducting pairing with a high momentum

The concept of SC pairing with a high momentum for a screened Coulomb repulsion [8] qualitatively corresponds to experimental data. In contrast to the models adjusted to describe low-energy excitations, it is based on a standard Hamiltonian that involves screening, the effect of the electron–phonon interaction, and the universality of the FC intrinsic in cuprates.

The shape of the FC of doped cuprates that agrees with the angle-resolved photoemission spectroscopy (ARPES) data in [29, 30] is described by the dispersion law

$$\varepsilon(\mathbf{k}) = -2t(\cos k_x + \cos k_y) + 2t' \cos k_x \cos k_y + t''(\cos 2k_x + \cos 2k_y)\,. \quad (1)$$

Here, the integrals of hopping between the nearest Cu atoms along the diagonal (t') and between the next-to-nearest Cu atoms in the direction of the Cu–O bond (t'') account for the fundamental asymmetry of the excitation spectrum (electron–hole asymmetry), which manifests itself, for example, in tunneling spectra [31].

The FC in Fig. 2 corresponds to the case where $t'/t \approx -0.3$ and $t''/t \approx 0.2$; these ratios correspond to the conditions that are optimal for superconductivity [4]. At a zero pair momentum, a logarithmic singularity occurs in the SC-pairing channel for any dispersion law, because $\varepsilon(\mathbf{k}) = \varepsilon(-\mathbf{k})$; therefore, the sensitivity of the SC state to the dispersion-law parameters indicates the specific features of the pairing kinetics in cuprates.

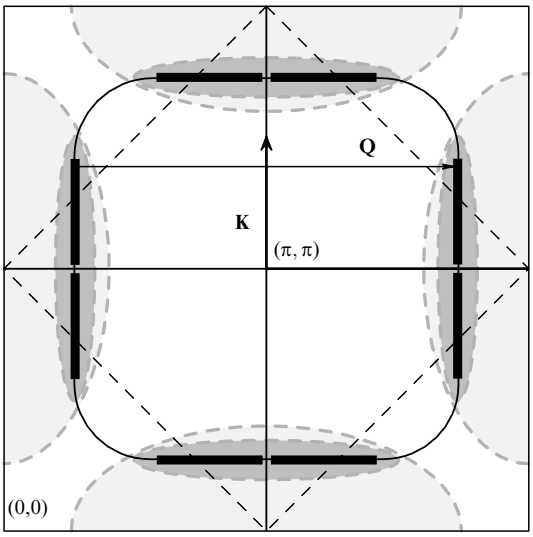

Figure 2. Fermi contour characteristic of underdoped cuprates (thin line). Heavy segments represent the parts of the FC in which mirror nesting occurs for pairs with the total momentum **K** and nesting occurs for pairs with the total momentum **Q**. Bright semiovals indicate the regions of the extended neighborhoods of saddle points, and dark semiovals correspond to the insulating pairing upon **K** pairing. The dashed line indicates the boundary of the magnetic Brillouin zone.

The almost rectilinear FC segments in an extended neighborhood of the saddle point symmetrically split with respect to the points $0, \pm\pi$ and $\pm\pi, 0$ (see Fig. 2) and lead to *nesting* $\varepsilon(\mathbf{k}+\mathbf{Q}) = -\varepsilon(\mathbf{k})$ for a certain incommensurate momentum $\mathbf{Q}$ that is not equal to the momentum (π, π) of the spin AF structure of the parent compound, and to a logarithmic singularity in the static generalized susceptibility $\chi(\mathbf{q})$ at $\mathbf{q} = \mathbf{Q}$, allowing instabilities in the insulating pairing channels. Apart from a spin density wave (SDW) with the AF vector $\mathbf{Q}$, a charge density wave (CDW), a charge current density wave (CCDW), and a spin current density wave (SCDW) can also appear. The insulating gap $\Delta_i(\mathbf{k})$ appears in a certain part of the FC, and dispersion law (1) transforms into the law

$$\varepsilon(\mathbf{k}) = \varepsilon_{1,2}(\mathbf{k}) = \varepsilon_+(\mathbf{k}, \mathbf{Q}) \pm \sqrt{\varepsilon_-^2(\mathbf{k}, \mathbf{Q}) + \Delta_i^2(\mathbf{k})}\,, \quad (2)$$

where $\varepsilon_\pm(\mathbf{k}, \mathbf{Q}) = \varepsilon(\mathbf{k}) \pm \varepsilon(\mathbf{k}+\mathbf{Q})$.

In the final portion (pair Fermi contour), the universal FC of cuprates satisfies the *mirror nesting* condition $\varepsilon(\mathbf{k}_+) = \varepsilon(\mathbf{k}_-)$ for a pair of particles (**K** pair) with momenta $\mathbf{k}_\pm = \mathbf{K}/2 \pm \mathbf{k}$ at a certain total momentum **K** (**k** is the momentum of the relative motion of the pair). This results in a logarithmic singularity in the SC pairing channel with the momentum **K** and the appearance of the following nontrivial solution of the self-consistency equation:

$$\Delta(\mathbf{k}) = -\frac{1}{2} \sum_{\mathbf{k}'} \frac{U(\mathbf{k}, \mathbf{k}')\, \Delta(\mathbf{k}')}{\sqrt{\xi^2(\mathbf{k}') + \Delta^2(\mathbf{k}')}}\,. \quad (3)$$

For pairing repulsion, the interaction energy is $U(\mathbf{k}, \mathbf{k}') > 0$ at any momenta $\mathbf{k}$ and $\mathbf{k}'$ before and after scattering, respectively. The nontrivial solution $\Delta(\mathbf{k})$ forms in the vicinity of the pair Fermi contour (PFC), in which the kinetic energy of a **K** pair $2\xi(\mathbf{k}) = \varepsilon(\mathbf{k}_+) + \varepsilon(\mathbf{k}_-)$ becomes zero or

almost zero owing to the competition of scattering inside regions of the same sign of $\Delta(\mathbf{k})$ and between these regions. As a result, we have to reverse the sign of the sum in Eqn (3). The coefficient of the logarithm in Eqn (3) is determined by the difference of the integrals over the momentum space regions where $\Delta(\mathbf{k})$ has different signs. In the absence of an electron–hole asymmetry, the pairing in the case of repulsion turns out to be substantially suppressed, whereas in the case of pairing attraction, the mirror nesting of the FC is sufficient for the appearance of an SC state in the weak-coupling limit. For the mirror nesting of the FC, the sufficient condition for the existence of a nontrivial solution of the self-consistency equation with pairing repulsion is the presence of at least one negative eigenvalue of the linear operator with the kernel $U(\mathbf{k}, \mathbf{k}')$.

For SC pairing with a nonzero pair momentum ($\mathbf{K}$ pairing), a *kinematic restriction* is imposed on the region of the momentum space where the particle momenta $\mathbf{k}_+$ and $\mathbf{k}_-$ can lie. The fact that the arguments $\mathbf{k}$ and $\mathbf{k}'$ of the pairing interaction kernel belong to the kinematically restricted region with a characteristic energy scale ε_0 means the elimination of the contributions of many scattering processes, especially those with large momentum transfers $\mathbf{k}' - \mathbf{k} \equiv \boldsymbol{\kappa}$, to the formation of the SC order parameter.

At small momentum transfers, the number of corresponding transitions inside the regions of the same sign of $\Delta(\mathbf{k})$ is approximately proportional to the areas of these regions, and the number of transitions changing the sign of the right-hand side of Eqn (3) is proportional to the area of a strip of the width $\varkappa$ and the length equal to the zero line length. Therefore, scattering with small momentum transfers strongly suppresses the amplitude of the solution of Eqn (3).

Particle scattering in an SC channel competes with phonon scattering, which is characterized by predominant transitions with relatively small momentum transfers. Phonon scattering decreases the contribution of scattering at small momentum transfers to the SC pairing interaction, which mainly occurs inside the momentum space region where $\Delta(\mathbf{k})$ has the same sign. This decrease in the scattering at small momentum transfers with repulsion favors an increase in T_c by weakening the effect of the thermal-excitation-induced breaking of pairs. The contribution of phonons to the pairing interaction due to the suppression of small momentum transfers under scattering is effective at energies lower than the characteristic phonon energy ω_D and disappears at higher energies. This behavior can cause a kink in the photoemission spectrum [32].

Nesting is accompanied by a scattering limitation at large momentum transfers, which is associated with the appearance of an insulating gap in almost rectilinear FC segments and the related redistribution of the spectral weight between the intersecting branches of the elementary-excitation spectrum [33]. When hole doping shifts the chemical potential toward the region below the lower edge of the insulating gap $2\Delta_i$, the spectral weight of the hole part (which is present in a small neighborhood of the lower-subband top) of the SC branch of the excitation spectrum decreases rapidly and passes from the SC branch to the insulating branch of the spectrum. This results in a suppression of the electron and hole momentum transfers that are significantly higher than $\mathbf{Q}$ during scattering. This *insulating limitation* of momentum transfer leads to an SC state with a small spectral weight.

A deviation from the mirror nesting can be taken into account by replacing almost rectilinear FC segments with straight-line segments at a given average deviation (on the energy scale δ) from the FC, i.e., by cutting off the logarithm from below: $\delta \leqslant \xi \leqslant \varepsilon_0$. The order parameter takes the form

$$\Delta(\mathbf{k}) = \operatorname{sgn} \Delta'(\mathbf{k}) \sqrt{\Delta'(\mathbf{k}) \left[\Delta'(\mathbf{k}) - \delta \operatorname{sgn} \Delta'(\mathbf{k})\right]}\,, \qquad (4)$$

where $\Delta'(\mathbf{k})$ is the solution of Eqn (3) at $\delta = 0$. The solution exists if $\delta < |\Delta'|$. As δ decreases, the order-parameter amplitude Δ formally increases, which is accompanied by a decrease in the PFC length and, hence, the amplitude Δ'. Thus, the amplitude Δ as a function of δ reaches its maximum, which corresponds to a certain pair momentum $\mathbf{K}$.

The singularity of the susceptibility $\chi(\mathbf{q})$ at $\mathbf{q} = \mathbf{Q}$ leads to the occurrence of a soft mode in the boson-excitation spectrum and the effective electron–electron interaction

$$V(\mathbf{q}) \approx \gamma^2\, \chi(\mathbf{q})\,, \qquad (5)$$

where γ has the meaning of a coupling constant that characterizes the interaction of electrons with the corresponding boson excitations. If $\chi(\mathbf{q})$ is the magnetic susceptibility, Eqn (5) describes the spin-fluctuation electron–electron interaction [34] for the appearance of an SDW with a momentum $\mathbf{Q}$. The singularity in the insulating susceptibility $\chi(\mathbf{q})$ corresponds to the Peierls instability [35]. During the nesting of the FC, the CCDW and SCDW related to the charge and spin current degrees of freedom lead to a singularity in the corresponding susceptibilities at $\mathbf{q} = \mathbf{Q}$ and to the electron–electron interaction of type (5). The coupling of a wave with an incommensurate period $2\pi/Q$ to the crystal lattice forms a commensurate structure with a similar period.

3. Superconducting order parameter

The restrictions on scattering at small and large momentum transfers can be taken into account by cutting off the screened pairing Coulomb interaction from below and from above: $q_l \leqslant \varkappa \leqslant q_r$. The numerical solution of Eqn (3) with such a model potential [36] demonstrates that the softening of the small momentum transfer limitation weakly affects the topological properties of the order parameter. For chosen dispersion law parameters, the amplitude Δ decreases sharply at a certain value of q_l, when the degree of the electron–hole asymmetry becomes insufficient to overcome the deviation of the FC from mirror nesting at a chosen coupling constant.

There exist two classes of solutions, which differ in symmetry with respect to a change in the sign of the projection of the relative motion momentum onto the nesting vector $\mathbf{Q}$ (i.e., symmetric and antisymmetric solutions). An antisymmetric solution with one node at the center of the kinematic limitation region corresponds to the maximum order-parameter amplitude. A symmetric solution with two nodes in the kinematic limitation region has a significantly lower amplitude. The antisymmetric solution with the next order-parameter amplitude has three nodes. A gradual decrease in the order-parameter amplitude corresponds to the alternation of the antisymmetric and symmetric solutions with a sequential increase in the number of nodes by unity. This resembles the node distribution of the wave function of a particle in a potential well in accordance with the oscillation theorem [37]; it should be noted that a node-free solution is absent in the case of repulsion. The degree of division of the kinematic limitation region depends on the pair momentum $\mathbf{K}$, which specifies the shape and size of this

region. As the kinematic limitation region extends along the axis normal to the nesting vector **Q**, the number of regions in which $\Delta(\mathbf{k})$ has a constant sign increases, the region size decreases, the order parameter is distributed between these regions, and its amplitude decreases. The amplitude Δ, which depends exponentially on the coupling constant and the kinematic limitation region parameters, is very sensitive to the choice of the dispersion law parameters and the level of doping.

At $K = 0$, an antisymmetric solution cannot be realized for singlet pairing, because it corresponds to the orbital p symmetry of the order parameter. A symmetric solution with two nodes and a significantly lower amplitude compared to the amplitude of the main solution leads to an order parameter with an extended s or d symmetry.

For the **K** pairing, an antisymmetric solution with the maximum order-parameter amplitude can be realized for each crystallographically equivalent pair momentum $\mathbf{K}_j$. The order parameter is small inside the intersection of different kinematic limitation regions and can be determined over the entire Brillouin zone as a linear combination of the solutions $\Delta_j(\mathbf{k})$ of Eqn (3) in each region,

$$\Delta(\mathbf{R}, \mathbf{k}) = \sum_j \gamma_j \exp(\mathrm{i}\mathbf{K}_j\mathbf{R})\, \Delta_j(\mathbf{k})\,, \tag{6}$$

where **R** is the center-of-mass radius vector of the **K** pair and the coefficients γ_j are determined by the irreducible representation used to transform order parameter (6). The irreducible representation A_{1g} results in the g symmetry of the order parameter with two families of zero lines, namely, along the coordinate axes and along the diagonals of the Brillouin zone. The representation B_{1g} corresponds to a d symmetry with zero lines along the coordinate axes. The symmetric solution with two nodes upon **K** pairing leads to an extended s symmetry in the case of the representation A_{1g} and to a d symmetry in the case of B_{1g}.

4. Biordered superconducting state and a strong pseudogap

The effective pairing potential $U(r)$ oscillates in real space due to the limitation of the domain of definition of the screened Coulomb repulsion $U(\mathbf{k}, \mathbf{k}')$ in the momentum space upon **K** pairing (Fig. 3). Strong repulsion at small distances corresponds to incomplete limitation of the double occupation [10]. Outside this region, damped oscillations naturally lead to an effective attraction, which is required for the appearance of a bound state in a **K** pair. Apart from the bound state with a negative energy E_i of the relative motion of a **K** pair, the oscillating pairing interaction allows long-lived QSSs of pairs with momenta close to **K**, which are similar to the states of radioactive isotopes exhibiting α decay. The wave functions of the relative motion of a **K** pair that correspond to the bound state and QSS are orthogonal to each other and are mainly localized in a wide real-space region outside the strong intracenter repulsion region (see Fig. 3). The presence of a tunneling barrier $E_b - E_q$ and orthogonal wave functions results in a pronounced asymmetry between the spectral weights of filled and vacant QSSs, which is reflected in the asymmetry of the tunneling current – voltage characteristics detected in [38, 39].

K pairs can exist as long-lived QSSs at temperatures above T_c owing to a significant increase in the density of states in a narrow range near the QSS energy E_q. To overcome a potential barrier before the tunneling decomposition of a

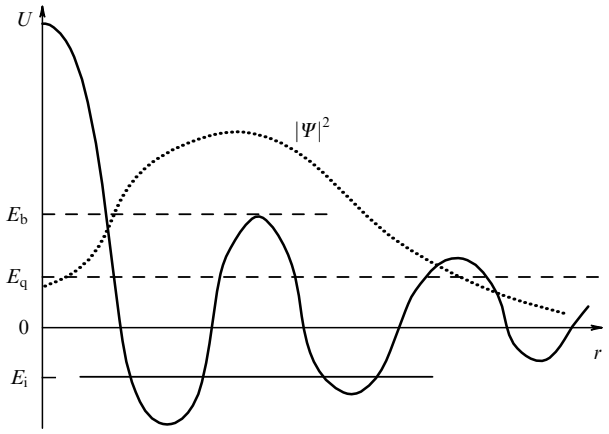

Figure 3. The oscillating pairing interaction $U(r)$ in real space and the squared modulus of the wave function of a **K** pair vs. the distance between the particles forming the pair. The BS and QSS energies of the pair are respectively denoted by E_i and E_q; E_b is the **K**-pair dissociation energy.

noncoherent pair, this pair should accumulate an energy higher than the barrier E_b. Thus, the energy $E_q - E_i$ is insufficient to destroy the SC coherence, and the pair breaking energy should exceed $E_b - E_i$. The range between the SC transition temperature $T_c \sim E_q - E_i$ and the crossover temperature $T_s^* \sim E_b - E_i$ can be interpreted as the strong pseudogap that is observed in underdoped cuprates at $T > T_c$. If the peak of the density of states at E_q is smoothed due to an increase in the QSS damping Γ, the strong pseudogap becomes undetectable. In this case, the SC transition from a coherent to a noncoherent state is accompanied by the breaking of pairs at energies about $E_b - E_i$, as in the BCS theory.

By analogy with the relation between the problem of two Cooper particles [40] and the BCS theory [2], the pair breaking energy $E_b - E_i$ for direct excitation from a bound state to a continuous spectrum corresponds to a momentum-dependent energy gap $\Delta(\mathbf{k})$ in the quasiparticle spectrum. For the strong-pseudogap state, this gap can be represented as $\Delta = (\Delta_c^2 + \Delta_p^2)^{1/2}$ due to the noncoherence of the QSS. Here, $\Delta_c \sim E_q - E_i$ corresponds to a transition into a noncoherent QSS state and $\Delta_p \sim E_b - E_q$ corresponds to a transition between two noncoherent states.

On the microscopic level of describing SC, the gap Δ_c and the strong pseudogap Δ_p appear with random phases. Taking the average in the mean-field approximation leads to the vanishing mean value of Δ_p at any temperature, whereas the mean value of Δ_c is nonzero for $T < T_c$ because of the Bose condensation of **K** pairs from a QSS into a bound state. The root-mean-square value of a strong pseudogap $|\Delta_p^2| \neq 0$ that corresponds to the decay of the QSS of **K** pairs can manifest itself at temperatures well above T_c.

We note that noncoherent SC pairs existing as a QSS for $T > T_c$ exhibit their SC properties (Fig. 4) in microwave superconductivity (at frequencies up to 600 GHz [41]) and magnetic properties (Fig. 5), i.e., an enhancement of the diamagnetic response and a giant Nernst effect [5–7].

In the mean-field approximation, the diagonal Gor'kov function phenomenologically introduced as [42]

$$G(\omega; \mathbf{k}) = z_{\mathbf{k}} \left[\frac{u_+^2(\mathbf{k})}{\omega - E(\mathbf{k}) + \mathrm{i}\Gamma} + \frac{u_-^2(\mathbf{k})}{\omega + E(\mathbf{k}) - \mathrm{i}\Gamma} \right] \tag{7}$$

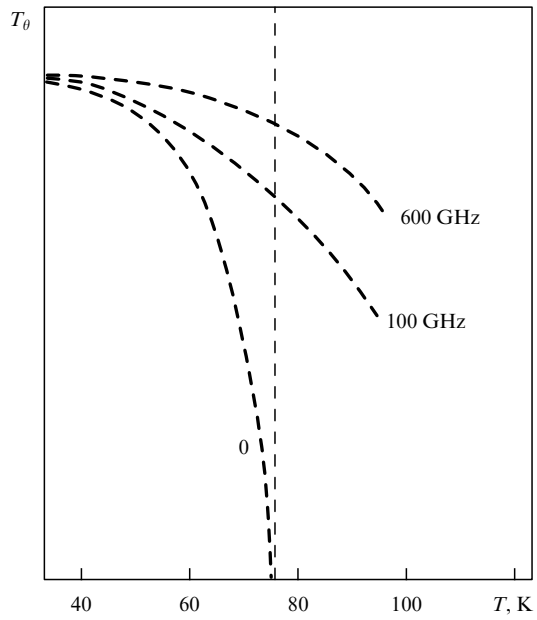

Figure 4. Temperature dependence of the phase rigidity (schematic diagram from the results of optical conductivity measurements [41]). Numerals at the curves are frequencies.

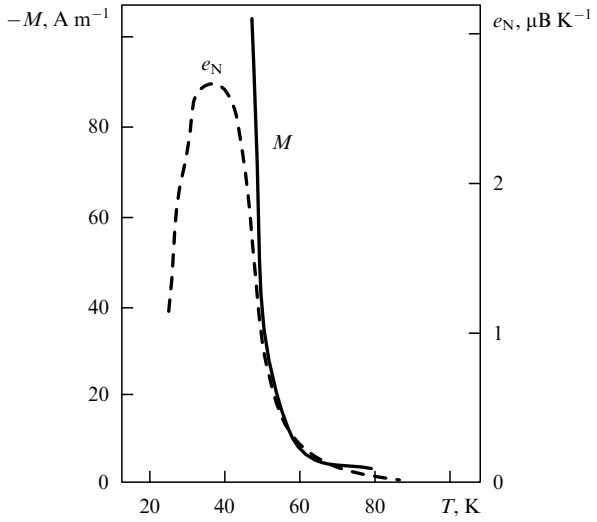

Figure 5. Diamagnetic response (magnetization M) and the Nernst signal e_N in an underdoped Bi-2212 compound (schematic diagram according to [5]).

describes a nonsuperconducting state with an *off-diagonal short-range order* (ODSRO) and corresponds to the presence of noncoherent pairs at $T > T_c$. Here, the quasiparticle energy is

$$E(\mathbf{k}) = \sqrt{\xi_K^2(\mathbf{k}) + |\Delta_c(\mathbf{k})|^2 + |\Delta_p(\mathbf{k})|^2}\,, \tag{8}$$

where $2u_\pm^2 = 1 \pm \xi_K/E$ are coherence factors and $z_\mathbf{k}$ is the momentum-dependent spectral weight of the quasiparticle. The terms in Eqn (7) pertain to pairs above and below the FC. At temperatures below T_c, an ODSRO transforms into an *off-diagonal long-range order* (ODLRO).

The excitation-induced transitions from a bound state to the QSS of the relative **K**-pair motion correspond to small but nonzero damping Γ, whereas the transitions to the stationary states of the continuous spectrum at energies higher than the barrier energy E_b should correspond to the infinitely small damping $\Gamma \to +0$. This leads to the usual Fermi-liquid behavior of diagonal Gor'kov function (7) for $T > T_s^*$ at $\Delta_p = 0$. Thus, as a result of the appearance of a QSS, the behavior of function (7) differs from the Fermi-liquid behavior over a rather wide temperature range of a strong pseudogap at $T < T_s^*$. This range corresponds to transitions between the bound and quasi-stationary states of **K** pairs and is intermediate between the two limiting approaches to the problem of superconductivity, the BCS scheme and the Bose–Einstein condensation of localized pairs. Because $|\Delta_p^2| \neq 0$ in the strong pseudogap state, the coherence factors in diagonal Gor'kov function (7) can overlap in the momentum space even at $T > T_c$, in contrast to the BCS factors (which have a Fermi shape).

The SC state appearing at $T < T_c$ should be described by both the diagonal and off-diagonal (anomalous) Gor'kov functions. We take into account that the strong pseudogap Δ_p averaged over random phases (i.e., corresponding to the mean-field approximation) vanishes (but $|\Delta_p^2| \neq 0$) and that $\Delta_c \neq 0$ at $T < T_c$, and phenomenologically introduce the anomalous Gor'kov function similarly to diagonal function (7),

$$F^+(\omega;\mathbf{k}) = -\frac{z_\mathbf{k}\Delta_c^*}{\bigl(\omega - E(\mathbf{k}) + i\Gamma\bigr)\bigl(\omega + E(\mathbf{k}) - i\Gamma\bigr)}\,. \tag{9}$$

This function becomes zero at $T > T_c$ and describes the ODLRO state at $T < T_c$.

In particular, superposition (6) mixes the states of two **K** pairs with opposite total momenta **K** and $-\mathbf{K}$. The particles making up these pairs can also form pairs with a nonzero total momentum, which relate the **K** pairing to the conventional Cooper pairing channel (at $K = 0$). In this case, the order parameters Δ_c and Δ_0 in the **K**-pairing and Cooper-pairing channels that correspond to the mean-field approximation are solutions of a set of self-consistency equations. This set decomposes into two independent equations if we neglect the relation between the channels, and determines two temperatures (T_c, T_c') of transitions to states with the respective order parameters Δ_c and Δ_0. It is natural to assume that $T_c' < T_c$, because an antisymmetric solution with the maximum order parameter is allowable upon singlet **K** pairing and because only a symmetric solution is realized in the Cooper channel. Then, the SC transition temperature T_c can be directly obtained from Eqn (3).

Both order parameters Δ_c and Δ_0 that describe a 'biordered' SC state [42, 43] are respectively determined in the neighborhoods of PFC and FC. At $T_c' \lesssim T < T_c$, the Cooper order parameter is small compared to Δ_0, since it is induced by the Δ_c pairing. In this temperature range, the superfluid density ρ_s is proportional to the PFC length. Opening the Cooper channel at $T \approx T_c'$ results in a substantial increase in Δ_0 and ρ_s, because superfluid density is proportional to the FC length at $T \lesssim T_c'$.

In the neighborhood of PFC, two branches ($m = 1, 2$) of the strongly anisotropic quasiparticle spectrum of a biordered superconductor take the form

$$E_m(\mathbf{k}) = \sqrt{\xi_K^2(\mathbf{k}) + |\Delta_p(\mathbf{k})|^2 + |\Delta_c(\mathbf{k}) \pm \Delta_0(\mathbf{k})|^2}\,. \tag{10}$$

The observation of a two-gap spectrum with Δ_1 and Δ_2 near 10 and 50 meV, respectively, in Bi-2212 in a tunneling

experiment (in particular, the suppression of the smaller gap in a strong magnetic field at temperatures 30 – 50 mK) [44] can be considered an argument for a biordered structure of the SC state.

The SC state of cuprates is biordered due to the specific features of their band structure that are associated with the CuO_2 plane and lead to the nesting and mirror nesting of the FC. The specific features of the phase diagram of cuprates (Fig. 1) can be related to the doping-induced evolution of the FC and pairing interaction. The $U(r)$ pairing potential, which oscillates in real space (see Fig. 3), is assumed to change with increasing x such that only a noncoherent QSS of the relative motion of a **K** pair appears in this potential at the weakest doping, which corresponds to a strong pseudogap penetrating into the insulating state at $x < x_*$. In the underdoped region ($x_* < x \lesssim x_{opt}$), a bound state of the pair appears along with the QSS, and the state energy E_i and the damping of the QSS Γ increase as x increases until, at x_{opt}, the pair breaking energy becomes approximately equal to the energy corresponding to the loss of phase coherence. Then, in the overdoped region ($x_{opt} \lesssim x < x^*$), the pairing interaction only causes a bound state, and superconductivity in this region of the phase diagram corresponds to the BCS scheme. As the degree of doping increases, the **K**-pairing channel gradually makes way for the Cooper channel, and, when x exceeds x_{opt}, the decrease in T_c with increasing x up to the vanishing of T_c at x^* can also be related to the doping dependence of the pairing interaction. Specifically, the enhancement of repulsion at $x > x_{opt}$ increases because the FC leaves the extended neighborhood of the saddle point.

The experimental data that are obtained for cuprates are unusual for the BCS scheme, and the phonon pairing mechanism can be naturally described using the concept of **K** pairing [8].

5. Superconductivity of multilayer cuprates

In the homologous series of cuprates, the SC transition temperature exhibits a universal dependence on the number n of CuO_2 planes in a unit cell. As n increases, the $T_c(n)$ function first increases and reaches a maximum at $n = 3$, and then decreases monotonically. Explaining the $T_c(n)$ dependence is a challenging problem of the physics of cuprates [17]. Figure 6 shows the $T_c(n)$ dependences of a number of mercury-containing cuprates [45].

The charge distribution introduced upon doping of multilayer compounds is nonuniform: the inner layers have a lower hole concentration compared to the outer layers, which corresponds to a minimum in the electrostatic energy [46]. The optimum doping of a multilayer compound consists in underdoped inner and overdoped outer planes, as compared to the optimum doping of a compound with a single CuO_2 plane in the unit cell.

Coherent tunneling of pairs between neighboring layers qualitatively (not quantitatively) explains the initial increase in the $T_c(n)$ function and its subsequent saturation (at $n > 3$) [47]. The decrease in $T_c(n)$ at $n > 3$ is explained by a nonuniform carrier distribution in unit-cell layers and the competition of an SC ordered state and an insulating (in the form of an orbital current density d wave) ordered state. The significant increase in the superconducting transition temperature with an increase in the number of unit-cell layers can be related to the fact that the effective radius of the screened Coulomb pairing interaction exceeds the distance between neighboring layers.

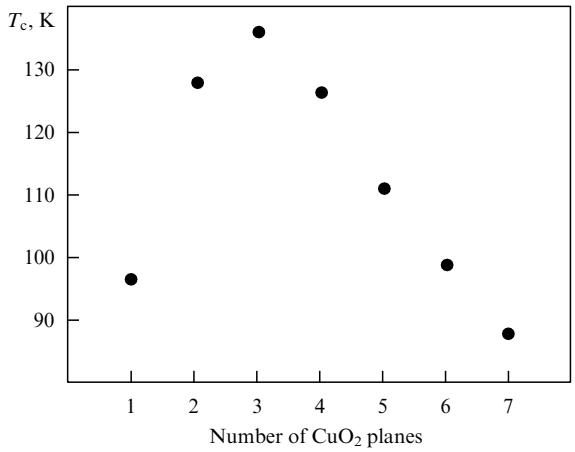

Figure 6. The SC transition temperature vs. the number of CuO_2 planes in a unit cell for the $HgBa_2Ca_{n-1}Cu_nO_{2n+2+\delta}$ homologous series (schematic diagram according to [45]).

The Fermi surface is open along the k_z axis because of the smallness of the hopping integrals between layers. The section of this surface by the k_xk_y planes corresponding to different layers represents a set of n layers, which are different due to different doping levels. SC pairing with momentum **K** can occur not only for the particle momenta $\mathbf{k}_\pm$ and $\mathbf{k}'_\pm$ (before and after scattering) in one plane but also in the case where these momenta correspond to different (nearest) planes. Another possibility is associated with pair tunneling between neighboring cuprate planes: particle momenta belong to one plane before scattering and to another plane after scattering.

With the **K**-pairing channel, we can easily explain the universal $T_c(n)$ dependence detected in the homologous series of cuprates.

The limitation related to taking the interaction into account only in the nearest neighbor layers reduces the increase rate of the effective coupling constant as n increases, since the inner layer has two nearest neighbors and the outer layers have only one nearest neighbor. If the FC were the same for all layers, the effective coupling constant would saturate as n increases. Nonuniform doping of cuprate layers within one unit cell violates the mirror nesting condition in the interlayer interaction mechanism, since the FCs of neighboring cuprate layers are different because of different degrees of their filling.

The difference in the carrier concentrations in neighboring layers plays the role of an exchange field in weakly ferromagnetic superconductors. The violation of the interlayer mirror nesting smooths the logarithmic singularity in the self-consistency equation and results in an order parameter of type (6), as in the case of the intralayer mirror nesting. The deviations from mirror nesting and the doping optimal for a monolayer increase with n because of an increase in the role of electrostatic effects, which reduce the condensation energy and are the main causes of the decrease in the $T_c(n)$ dependence after reaching its maximum.

Cuprates are strongly anisotropic quasi-two-dimensional systems of weakly coupled CuO_2 planes; therefore, cuprate superconductivity theories are constructed as theories describing one such plane. In crystals with several weakly tunneling-coupled CuO_2 planes, the Coulomb pairing interaction only couples pairs of the nearest-neighbor planes because of the specific features of 2D screening [50]. There-

fore, an increase in the number of layers in a unit cell results in a noticeable increase in the effective coupling constant only at small n; for $n > 3$, this increase slows down and the coupling constant saturates. The presence of charge reservoirs between conducting planes in multilayer cuprates, which favors superconductivity in the CuO_2 plane in the sense that doping does not cause structural defects in it, leads to a nonuniform carrier distribution in unit-cell planes, which is required for the minimization of the electrostatic energy. In the case of **K** pairing (where an antisymmetric solution corresponding to the maximum possible SC order parameter amplitude), the role of this nonuniform distribution, which violates the mirror nesting of the FC upon pairing in neighboring layers, is analogous to the role of magnetization, which changes the pairing conditions and decreases T_c.

6. Increasing the superconducting transition temperature: the 3D path

The search for or creation of structures with SC transition temperatures higher than the reached record value can be related to the variation in the chemical compositions and structures of cuprate superconductors. The estimates made in terms of the $t-J$ model suggest that layered 2D cuprate-like compounds in which Cu atoms in conducting planes are replaced by any other elements that can supply carriers to these planes can hardly exhibit the T_c characteristics of cuprates [28]. This means that the path of a significant increase in T_c due to a change in the chemical composition of conducting planes in such 2D crystals is most likely to be a traveled path. Nevertheless, the substantial increase in T_c in multilayer cuprates (compared to T_c in the corresponding one-layer cuprates) at $1 < n \lesssim 3$ indicates the possibility of enhancing the effective coupling constant in passing from a 2D to a 3D (three-dimensional) system and another, apparently more promising, way of searching for high-T_c compounds.

The realization of the **K**-pairing conditions in a 3D system is mainly restricted by how close the Fermi surface (FS) can approach the mirror nesting condition in a sufficiently wide 3D kinematic limitation region. If we start with the dispersion law characteristic of strongly coupled cuprates, it is obvious that mirror nesting for such a structure can be provided if certain relations between the dispersion-law parameters are satisfied. Therefore, the main problem is to control these parameters such that they fall in relatively narrow ranges corresponding to mirror nesting.

When atoms form a simple cubic lattice, the dispersion law that takes hopping only between the nearest, next-to-nearest, and next-next-to-nearest neighbor atoms into account is

$$\begin{aligned}\varepsilon(k_x,k_y,k_z) = {} & -2t(\cos k_x + \cos k_y + \cos k_z) \\ & + 2t'(\cos k_x \cos k_y + \cos k_y \cos k_z + \cos k_z \cos k_x) \\ & + t''(\cos 2k_x + \cos 2k_y + \cos 2k_z)\,. \end{aligned} \tag{11}$$

It leads to a large variety of FS shapes, depending on the chemical potential. In particular, the FS can have the shape of a cube with rounded corners and weakly bent faces parallel to the boundaries of the 3D Brillouin zone. At the hopping-integral ratios $t'/t \approx -0.3$ and $t''/t \approx +0.3$ [which differ from the ratios characteristic of 2D cuprates ($t'/t \approx -0.3$, $t''/t \approx +0.2$)], this FS provides nesting at momenta **Q** connecting the faces and mirror nesting at pair momenta **K** parallel and not equal to **Q**. As in the case of large-momentum pairing in a 2D system, the 3D kinematically restricted regions that appear in the case of **K** pairing result in a screened pairing Coulomb potential that oscillates in real space and extends outside the region of strong intracenter repulsion. This potential, one of whose eigenvalues is negative, allows the existence of bound states of both the relative motion of a pair and the QSS.

The conditions for the occurrence of a bound state in an asymmetric 3D potential well differ from those for low-dimensional systems [37]: generally speaking, a 3D potential well couples a pair of particles weakly compared to a 2D well with the same depth and width. However, upon **K** pairing in a 3D system with the mirror nesting of the FS, a logarithmic singularity forms in the self-consistency equation in the neighborhood of the part of the Fermi surface where the mirror nesting condition is satisfied rather than in the neighborhood of a line in the Fermi surface, as in a 2D system (where this line is represented by the PFC). For a pair momentum directed along a Brillouin zone edge, this part (*pair Fermi surface,* PFS) includes two pairs of mutually perpendicular planar FC sections connected by rounded portions of the PFS (Fig. 7) rather than one pair of parallel planar FS sections, as in the case of **K** pairing in a 2D system (where the PFC consists of two parallel FC segments). This corresponds to an increase in the density of states of the relative motion of a **K** pair on the FS, which is tantamount to an increase in the effective coupling constant. Thus, upon **K** pairing, any section of the FS by a plane normal to the pair momentum inside the kinematic limitation region satisfies the mirror nesting condition (e.g., for a section by the (k_x, k_y) plane, pairing with a momentum $\mathbf{K} = (0, 0, K)$ is similar to the Cooper pairing that corresponds to the zero projection of the pair momentum onto this plane), and the role of almost planar FS faces is to ensure as large a PFS area as possible.

The nesting condition that favors insulating pairing at nesting momentum **Q** that is normal to only one pair of the FS face pairs is also satisfied at almost planar FS faces, although both pairs of faces promote SC pairing. In this sense, the efficiency of insulating pairing with respect to SC pairing in a 3D system decreases compared to that in a 2D system; that is, the appearing SC order is suppressed more weakly by a competing insulating order.

The repulsion-induced pairing in a 3D system leads to the SC order parameter $\Delta(\mathbf{K})$ with zeros distributed over the *zero surface* that has lines of intersection with the FS and corresponds to the symmetry or antisymmetry of $\Delta(\mathbf{K})$ with respect to the inversion of the momentum of the relative motion of a pair. The coefficient of the logarithm in the self-consistency equation is specified by the neighborhood of the

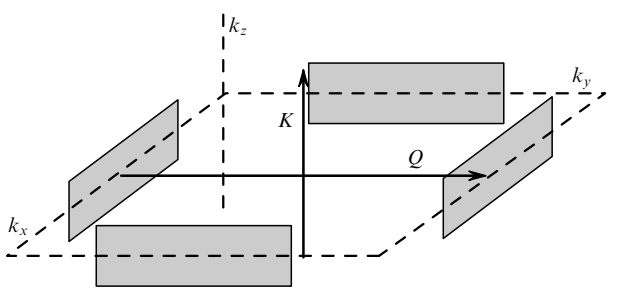

Figure 7. Nesting (at momentum **Q**) and mirror nesting (at total pair momentum **K**) for a Fermi surface with almost planar sections (shaded).

line of intersection of the FS and the order parameter zero line in which both intersecting surfaces are close to each other. For a d-wave order parameter in a 2D system, these neighborhoods of the points of intersection of the FC and the zero line along the diagonals of the Brillouin zone are definitely small, which strongly restricts the SC gap amplitude, e.g., in the scheme of spin-fluctuation pairing [34]. Therefore, the more complex topology of the SC order parameter, which results from **K** pairing upon Coulomb repulsion and is determined by the distribution of zero lines or surfaces in a 2D or 3D system, can lead to a substantially larger gap.

The complex topology of the momentum-dependent SC order parameter that is inherent in repulsion-induced pairing significantly complicates the numerical solution of a 2D self-consistency equation [36], e.g., compared to the corresponding procedure in the Eliashberg theory [21], where the order parameter depends on a single energy variable.

Of course, the ideology of the physics of cuprates cannot be used to search for or to create high-T_c 3D systems. If superconductivity in such a system is assumed to be realized upon doping of a certain parent insulator (as in the case of cuprates), the problem of a charge reservoir for a 3D atomic lattice supplying carriers to the conduction band appears. If superconductivity in a 3D crystal occurs in the absence of doping for a not-half-filled conduction band, the problem of controlling the dispersion-law parameters in a given crystal structure in order to ensure the mirror nesting of the FS is still an open question.

Because the superfluid density in underdoped cuprates is low, the phase transition into an SC state, i.e., the appearance of phase coherence, is specified not by the SC pair binding energy but by phase fluctuations [51]. Therefore, an SC transition in a 2D system inevitably acquires the features of the Berezinskii – Kosterlitz – Thouless transition [52, 53], which describes the thermal birth and disappearance of vortex – antivortex pairs. In a 3D system, the SC transition temperature is much less sensitive to phase fluctuations, which should broaden the SC state region due to the narrowing of the strong-pseudogap region, whose size increases with decreasing the vortex core energy [4].

Acknowledgments. This work was supported by the Russian Foundation for Basic Research, project nos. 05-02-17077a, 06-02-17186a.

References

1. Bednorz J G, Müller K A *Z. Phys. B* **64** 189 (1986)
2. Bardeen J, Cooper L N, Schrieffer J R *Phys. Rev.* **108** 1175 (1957)
3. Norman M R, Pines D, Kallin C *Adv. Phys.* **54** 715 (2005)
4. Lee P A, Nagaosa N, Wen X-G *Rev. Mod. Phys.* **78** 17 (2006)
5. Wang Y et al. *Phys. Rev. Lett.* **95** 247002 (2005)
6. Li L et al. *Europhys. Lett.* **72** 451 (2005)
7. Wang Y, Li L, Ong N P *Phys. Rev. B* **73** 024510 (2006)
8. Belyavsky V I, Kopaev Yu V *Usp. Fiz. Nauk* **176** 457 (2006) [*Phys. Usp.* **49** 441 (2006)]
9. Izyumov Yu A *Usp. Fiz. Nauk* **161** (11) 1 (1991); **165** 403 (1995); **169** 225 (1999) [*Sov. Phys. Usp.* **34** 935 (1991); *Phys. Usp.* **38** 385 (1995); **42** 215 (1999)]
10. Laughlin R B, cond-mat/0209269 (unpublished)
11. Franck J P, Lawrie D D *J. Supercond.* **8** 591 (1995)
12. Zhao G et al. *Nature* **385** 236 (1997)
13. Williams G V M et al. *Phys. Rev. Lett.* **80** 377 (1998)
14. Zhao G *Phys. Rev. B* **64** 024503 (2001)
15. Brandow B H *Phys. Rev. B* **65** 054503 (2002)
16. Basov D N, Timusk T *Rev. Mod. Phys.* **77** 721 (2005)
17. Leggett A J *Nature Phys.* **2** 134 (2006)
18. Loram J W et al. *Physica C* **341 – 348** 831 (2000)
19. Orenstein J, Millis A J *Science* **288** 468 (2000)
20. Demler E, Hanke W, Zhang S-C *Rev. Mod. Phys.* **76** 909 (2004)
21. Maksimov E G *Usp. Fiz. Nauk* **170** 1033 (2000) [*Phys. Usp.* **43** 965 (2000)]
22. Anderson P W *Science* **235** 1196 (1987)
23. Anderson P W et al. *J. Phys.*: *Condens. Matter* **16** R755 (2004)
24. Franz M, Tešanović Z, Vafek O *Phys. Rev. B* **66** 054535 (2002)
25. Sachdev S *Science* **288** 475 (2000)
26. Zhang S-C *Science* **275** 1089 (1997)
27. Guidry M et al. *Phys. Rev. B* **63** 134516 (2001)
28. Lee P A *Rep. Prog. Phys.* **71** 012501 (2008)
29. Campuzano J C, Norman M R, Randeria M, in *The Physics of Superconductors* Vol. 2 *Superconductivity in Nanostructures, High-T_c and Novel Superconductors, Organic Superconductors* (Eds K H Bennemann, J B Ketterson) (Berlin: Springer-Verlag, 2004) p. 167
30. Damascelli A, Hussain Z, Shen Z-X *Rev. Mod. Phys.* **75** 473 (2003)
31. Hirsch J E *Phys. Rev. B* **59** 11962 (1999)
32. Lanzara A et al. *Nature* **412** 510 (2001)
33. Rusinov A I, Kat D C, Kopaev Yu V *Zh. Eksp. Teor. Fiz.* **65** 1984 (1973) [*Sov. Phys. JETP* **38** 991 (1974)]
34. Millis A J, Monien H, Pines D *Phys. Rev. B* **42** 167 (1990)
35. Bulaevskiĭ L N *Usp. Fiz. Nauk* **115** 263 (1975) [*Sov. Phys. Usp.* **18** 131 (1975)]
36. Belyavsky V I, Kapaev V V, Kopaev Yu V *Pis'ma Zh. Eksp. Teor. Fiz.* **86** 462 (2007) [*JETP Lett.* **86** 404 (2007)]
37. Landau L D, Lifshitz E M *Kvantovaya Mekhanika*: *Nerelyativistskaya Teoriya* (Quantum Mechanics: Non-Relativistic Theory) (Moscow: Fizmatlit, 2001) [Translated into English (Oxford: Pergamon Press, 1977)]
38. Pan S H et al. *Nature* **413** 282 (2001)
39. Randeria M et al. *Phys. Rev. Lett.* **95** 137001 (2005)
40. Cooper L N *Phys. Rev.* **104** 1189 (1956)
41. Corson J et al. *Nature* **398** 221 (1999)
42. Belyavsky V I, Kopaev Yu V *Phys. Rev. B* **76** 214506 (2007)
43. Belyavskiĭ V I, Kopaev Yu V, Nguen Ngoc Tuan *Zh. Eksp. Teor. Fiz.* **132** 831 (2007) [*JETP* **105** 726 (2007)]
44. Vedeneev S I, Maude D K *Phys. Rev. B* **72** 144519 (2005)
45. Kuzemskaya I G, Kuzemsky A L, Cheglokov A A *J. Low Temp. Phys.* **118** 147 (2000)
46. Trokiner A et al. *Phys. Rev. B* **44** 2426 (1991)
47. Chakravarty S, Kee H-Y, Völker K *Nature* **428** 53 (2004)
48. Chakravarty S et al. *Phys. Rev. B* **63** 094503 (2001)
49. Belyavsky V I, Kopaev Yu V *Pis'ma Zh. Eksp. Teor. Fiz.* **83** 606 (2006) [*JETP Lett.* **83** 515 (2006)]
50. Ando T, Fowler A B, Stern F *Rev. Mod. Phys.* **54** 437 (1982)
51. Emery V J, Kivelson S A *Nature* **374** 434 (1995)
52. Berezinskii V L *Zh. Eksp. Teor. Fiz.* **61** 1144 (1971) [*Sov. Phys. JETP* **34** 610 (1972)]
53. Kosterlitz J M, Thouless D J *J. Phys. C*: *Solid State Phys.* **6** 1181 (1973)